Technical Paper
J. Astron. Space Sci. 32(4), 427-434 (2015)
http://dx.doi.org/10.5140/JASS.2015.32.4.427

JASS Journal of Astronomy and Space Sciences

Installation of Induced Current Measurement Systems in Substations and Analysis of GIC Data during Geomagnetic Storms

Kyu-Cheol Choi[1†], Mi-Young Park[1], Youngsoo Ryu[1], Youngsu Hong[1], Jong-Hyuk Yi[1], Sung-Won Park[2], Jae-Hun Kim[2]

[1]Research Institute, SELab, Seoul 06049, Korea
[2]Korean Space Weather Center, National Radio Research Agency, Jeju 63025, Korea

Coronal Mass Ejections (CME), which originate from active regions of the Sun's surface, e.g., sunspots, result in geomagnetic storms on Earth. The variation of the Earth's geomagnetic field during such storms induces surface currents that could cause breakdowns in electricity power grids. Hence, it is essential to both monitor Geomagnetically Induced Currents (GICs) in real time and analyze previous GIC data. In 2012, in order to monitor the variation of GICs, the Korean Space Weather Center (KSWC) installed an induced current measurement system at SINGAPYEONG Substation, which is equipped with 765 kV extra-high-voltage transformers. Furthermore, in 2014, two induced current measurement systems were installed on the 345 kV high-voltage transformers at the MIGEUM and SINPOCHEON substations. This paper reports the installation process of the induced current measurement systems at these three substations. Furthermore, it presents the results of both an analysis performed using GIC data measured at the SINGAPYEONG Substation during periods of geomagnetic storms from July 2013 through April 2015 and the comparison between the obtained GIC data and magnetic field variation (dH/dt) data measured at the Icheon geomagnetic observatory.

Keywords: induced current measurement system, geomagnetically induced current (GIC), geomagnetic storm

1. INTRODUCTION

Solar flares and coronal mass ejections, resulting from solar activities, cause geomagnetic storms that have effects on the Earth's magnetic field (Moon et al. 2002; Wang et al. 2002; Cho et al. 2004; Kim et al. 2008; Rho & Chang 2008, 2009). Geomagnetic storms represents the solar activity conditions (Oh & Kim 2013). Geomagnetic storms are an important part of the space weather forecast (Kim & Chang 2014). Geomagnetic storms can cause disruptions in communications, GPS, satellites, geological explorations, and power grids and affect pipage and steel cables (Sung & Lee 1998). Many socioeconomic activities rely on these systems or products and increasing levels of effort have been expended on preventing the damage caused by geomagnetic storms (Ahn 2000; Choi et al. 2005). Among these disruptions, the induced currents caused by geomagnetic storms can have considerable effect on power grids in high-latitude regions; in particular, long power lines and high-voltage transformers are highly vulnerable (Kappenman et al. 1981; Kappenman 2000; Boteler 2001; Park & Ryu 2013). For example, the power grid attack that occurred in Quebec (Canada) on March 13, 1989, resulted in the blackout of six million homes and considerable economic losses (Boteler et al. 1989; Kappenman 2000; Boteler 2001). In the same period, power transformers in New Jersey (USA) were damaged and their repair took over six weeks. During the powerful geomagnetic storm of October 29–30, 2003, southern Sweden experienced a 20–50 min power grid blackout, and 15 transformers were damaged in South Africa at the same time. Geomagnetic disruptions due to geomagnetic storms induce direct currents on extended power lines that can flow into transformers.

Received Nov 5, 2015 **Revised** Nov 25, 2015 **Accepted** Nov 27, 2015
†**Corresponding Author**
E-mail: kcchoi@selab.co.kr, ORCID: 0000-0002-0056-5293
Tel: +82-2-3447-9714, Fax: +82-2-878-1971

Depending on the strength and duration of such induced currents, disconnection or overload of transformers could occur. Recently, it has been reported that large-scale geomagnetic storms induce currents in mid- or low-latitude areas and thus, in China, Japan, and South Africa, which are in mid- and low-latitude areas, active research has been conducted on protecting national power grids against powerful geomagnetic storms (Park 2013).

In 2012, in Korea, for the protection of power grids, the Korean Space Weather Center (KSWC) of the National Radio Research Agency (RRA) established an induced current measurement system at SINGAPYEONG Substation, which is equipped with 765 kV extra-high-voltage transformers. Subsequently, two other induced current measurement systems were installed at MIGEUM and SINPOCHEON substations, which are both equipped with 345 kV high-voltage transformers. The measured induced currents are collected and analyzed at the data acquisition PC and these data are transmitted to the KSWC in Jeju. In this paper, the installation process of the induced current measurement systems at the three substations is summarized. Furthermore, the Geomagnetically Induced Current (GIC) data measured at the SINGAPYEONG Substation during periods of geomagnetic storms are analyzed. Comparison is made between the obtained GIC data and magnetic field variation (dH/dt) data measured at the Icheon geomagnetic observatory, which is the closest such facility to SINGAPYEONG Substation.

2. INSTALLATION OF INDUCED CURRENT MEASUREMENT SYSTEM

2.1 Induced Current Measurement System

The induced current measurement system, installed by the KSWC at each of the three substations, comprises a sensor system, data transfer system, and data storage system (Fig. 1). A clamp device is installed to the sensor to measure the induced currents on the neutral ground wire of a transformer. The data transfer system converts the measured analog signals into digital signals and transmits those data to the data acquisition PC. The data storage system utilizes a PC both to store the measured data and to transmit the data to the server system of the KSWC at Jeju. For the transmission of these data and for server security, a Virtual Private Network (VPN) system was installed. The list of the installed equipment is shown in Table 1.

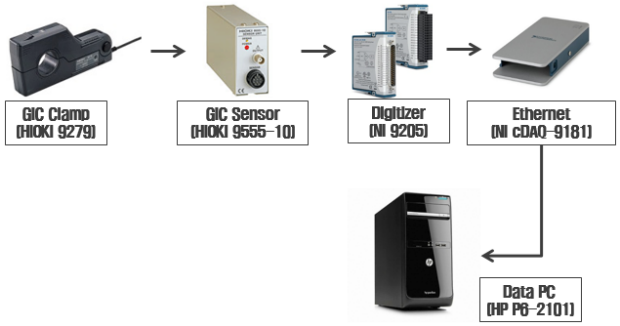

Fig. 1. Block diagram of induced current measurement equipment.

2.2 Installation of Induced Current Measurement System at the Three Substations

2.2.1 SINGAPYEONG Substation

SINGAPYEONG Substation is equipped with transformers of the highest domestic rating (765 kV) and it is one of the substations crucial to the supply of power to the Seoul metropolitan area. SINGAPYEONG Substation is linked to the SINTAEBAEK Substation with long power cables and the capacity of its transformer is large; thus, it is prone to the effects of induced currents generated by geomagnetic storms. Should this substation fail, the metropolitan area could suffer considerable damage. In order to both study the impact of induced currents on the transformer and prepare for failures of the transformers, the KSWC installed an induced current measurement system at the SINGAPYEONG Substation in 2012.

The measuring sensor is deployed externally to measure the induced currents on the neutral ground wire of the 765 kV extra-high-voltage transformer, and an enclosure unit has been installed to protect the sensor system. The

Table 1. Equipment classification

NO	Classification	Model	Quantity	Note
1	GIC Clamp &Sensor	HIOKI 9279/9555-10	1	Outside
2	Digitizer	NI 9205 32-Channel	1	Outside
3	Ethernet Chassis	NI cDAQ-9181	1	Outside
4	PC	HP Pavilion P6-2101KL	2	Indoor, Jeju
5	Sensor housing	Custom order	1	Outside
6	Installation Accessory	Table, Multitap	1	
7	Network Accessory	Line-sharer, Optical converters, Optical cable, LAN cable	1	

enclosure unit is made of stainless steel and it contains the GIC clamp, sensor unit, digitizer (to transfer data), and Ethernet chassis. Fig. 2 shows the sensor of the induced current measurement system and its enclosure unit. Measured induced current data are transmitted via Ethernet cable to the data acquisition PC, which is located in the second field control room. The acquired data are sent to the KSWC via the Internet network installed in the computer room of the main building; optical cabling is used to minimize data losses during transmission.

2.2.2 MIGEUM Substation

Because 345 kV high-voltage transformers are similarly prone to the effects of induced currents, an induced current measurement system was also installed at the MIGEUM Substation, which is linked to the SINGAPYEONG Substation. The neutral ground wire is used to measure the induced currents at the MIGEUM Substation. It is laid inside the shielding wall of the transformer, located at a height of 7 m; thus, the induced current measurement system is installed at the uppermost region of the shielding wall. In order to protect the induced current measurement system, an enclosure unit made of stainless steel has been installed. The enclosure unit is fixed on the shielding wall and it contains the component devices, other than the measurement sensor. The measurement sensor is enclosed in a protective case separate to the enclosure unit. For durability, both the enclosure unit and sensor protection case are made of stainless steel and they are connected by a flexible 28 mm aluminum pipe. After the power cable and optical cable (for transmitting signals) were inserted into the enclosure unit, the operational devices were set up. After the installation was completed and power applied, the sensor was connected to the neutral ground wire and tests were performed to ensure that the measured induced currents were received and displayed properly by the data acquisition PC. After data acquisition had been verified, the sensor protection case was sealed with silicon to prevent intrusion by rainwater. Fig. 3 displays the enclosure unit and sensor protection case.

A PC, used to store the measured induced current data and to transmit these data to the KSWC was installed in the machine room, and a rack was installed for the security and protection of the PC. The Internet network was installed in the communication room , which was linked to the data acquisition PC and the communication room via a LAN cable. In addition, for the security of the data transfer, a VPN system was installed in the rack and the transmission of data to both the KSWC and the display were verified as functioning properly. Fig. 4 shows the data acquisition PC installed in the communication room and a real-time image of the executable program.

2.2.3 SINPOCHEON Substation

Similar to the MIGEUM Substation, the SINPOCHEON Substation has high-voltage transformers (345 kV) and it supplies power to the area of northern Seoul. The process of installation of the induced current measurement system here was the same as at the MIGEUM Substation. The induced current measurement sensor is installed at the top of the transformer-shielding wall at a height of 7 m. Here, too, a stainless steel enclosure unit has been installed to protect the sensor.

Fig. 5 shows the enclosure unit and the flexible pipe protecting the induced current measurement equipment.

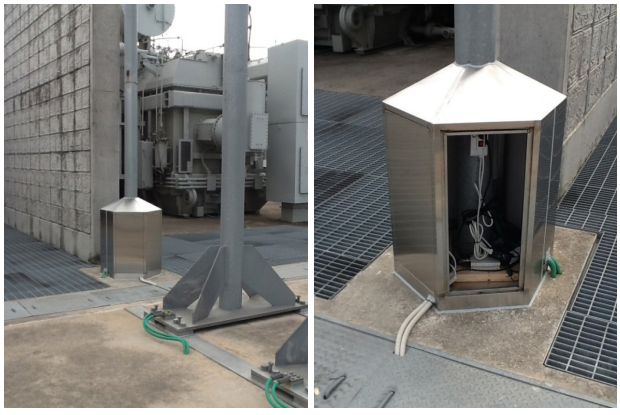

Fig. 2. Protective enclosure and sensor at SINGAPYEONG Substation.

Fig. 3. Protective enclosure and sensor case at MIGEUM Substation.

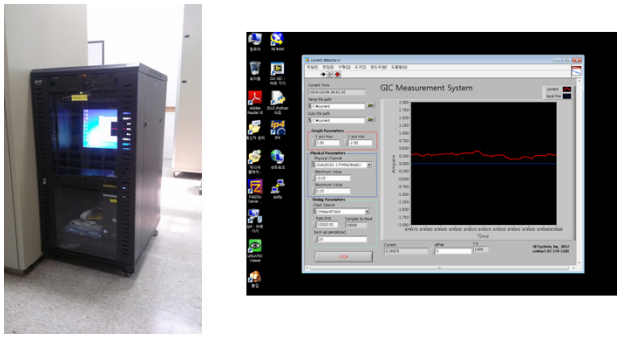

Fig. 4. Data acquisition PC and executable program at MIGEUM Substation.

The data acquisition PC and the VPN have been installed in the communication room on the first floor of the main building. Here, too, a rack was installed to protect the equipment, and the data are transmitted to the KSWC via the KT Internet network. Fig. 6 shows the installed data acquisition PC and a real-time image of the executable program.

3. ANALYSIS OF INDUCED CURRENT AND GEOMAGNETIC VARIATION DURING PERIODS OF GEOMAGNETIC STORMS

3.1 Selection of Geomagnetic Storm Events

Domestic research on GICs is lacking. Therefore, in this study, analysis was performed for periods of geomagnetic storms using the measurements of induced currents obtained from the induced current measurement system of the SINGAPYEONG Substation. For the analysis of GIC during geomagnetic storm periods, geomagnetic storms were selected among those occurred during the period from July of 2013 to April 2015. During this time, the periods showing the minimum value of SYM-H index below -50 nT were selected and in order to identify geomagnetic storms, SYM-H index which is indicating the intensity of the geomagnetic storms (Park et al. 2015) and Interplanetary Magnetic Field (IMF) and plasmas data time-shifted to the nose of the Earth's bow shock and magnetic indices were used. Fig. 7 shows the geomagnetic storm occurred from March 17-18, 2015. The figure shows the magnitude of magnetic field (IMF |B|), Bz component of IMF, solar wind speed (Vsw), solar wind density, solar wind temperature, AE index and SYM-H index from the top. This was a strong geomagnetic storm which showed - minimum value of SYM-H index, -234 nT.

In this research, the period of a geomagnetic storm is defined as the time of the storm sudden commencement(in Fig. 7. ① on SYM-H index) to the time when the value of the SYM-H index recovers to 60% of its minimum value(in Fig. 7. ② on SYM-H index). Of the periods selected, those indicating mechanical failure of the induced current measurement system and geomagnetic field measurement system were removed, which left 11 geomagnetic storm events for the analysis. The start and end times of the geomagnetic storms and the minimum values of the SYM-H

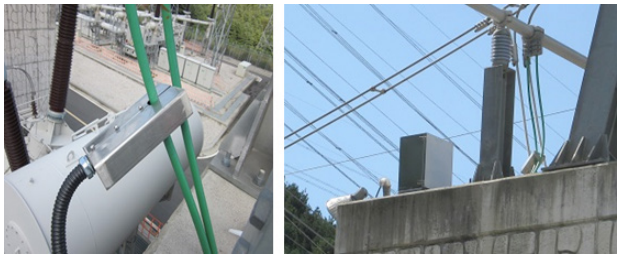

Fig. 5. Protective enclosure and sensor case at SINPOCHEON Substation.

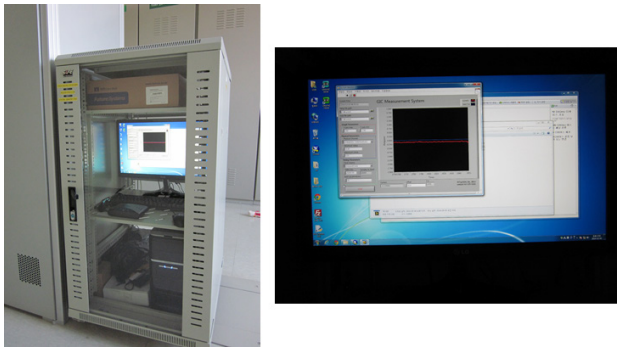

Fig. 6. Data acquisition PC and executable program at SINPOCHEON Substation.

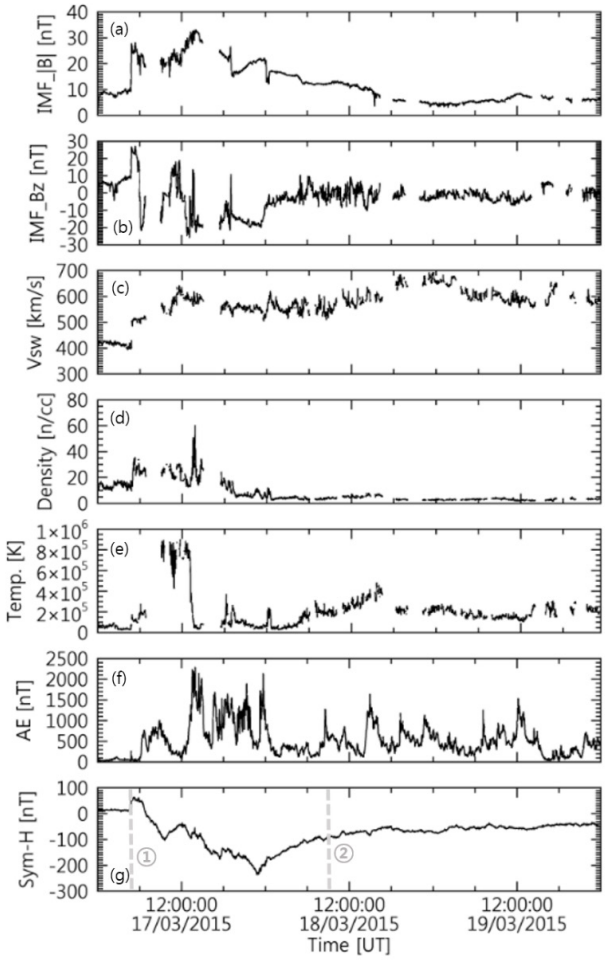

Fig. 7. (a) Magnitude of the magnetic field (IMF |B|), (b) Bz component of the IMF, (c) solar wind speed (Vsw), (d) solar wind density, (e) solar wind temperature, (f) AE index, and (g) SYM-H index of the geomagnetic storm event on March 17–19, 2015.

index for event are summarized in Table 2. An analysis of the measured GIC data and the geomagnetic field variation (dH/dt) data for these 11 events was performed.

3.2 Analysis

To analyze the domestically measured GIC and dH/dt data, the GIC data obtained at the SINGAPYEONG Substation were converted from 1 sec to 1 min resolution and the magnetic field data, measured at the Icheon geomagnetic observatory, were converted from 1 sec to 1 min resolution to calculate dH/dt. Fig. 8(a)–8(d) shows the GIC data [A], dH/dt [nT/min], AE index [nT], and SYM-H index [nT], respectively, of the geomagnetic storm that occurred on June 8–9, 2014. It can be seen that both the GIC and the dH/dt data fluctuate slightly at first and then, the amplitudes of their fluctuations increase considerably at around the minimum value of the SYM-H index. The dH/dt data fluctuate slightly in the range of -2 to 2 nT/min at first before the amplitude of the variation increases up to -10 to 15 nT/min at around the minimum value of the SYM-H index. The GIC data fluctuate slightly in the range of -1 to 1 A before the amplitude of the variation increases to -5 to 4 A when the value of dH/dt increases.

Table 2. List of geomagnetic storm events

Geomagnetic storm start time (UT)	Geomagnetic storm end time (UT)	SYM-H index Minimum value
2013-07-05 18:04	2013-07-07 04:33	-80
2013-10-08 20:25	2013-10-09 19:56	-77
2013-12-07 22:41	2013-12-08 23:49	-72
2014-02-18 13:25	2014-02-22 06:46	-127
2014-02-27 16:55	2014-03-01 11:14	-101
2014-04-11 05:26	2014-04-13 23:07	-92
2014-04-29 21:53	2014-05-01 04:59	-76
2014-06-07 16:56	2014-06-09 08:30	-72
2015-02-14 22:04	2015-02-19 06:58	-70
2015-03-17 04:48	2015-03-18 08:48	-234
2015-04-09 21:51	2015-04-11 20:12	-89

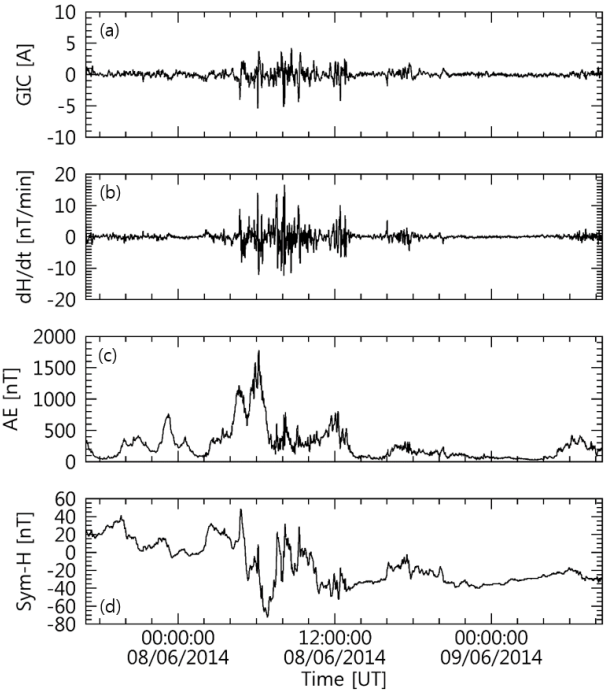

Fig. 8. (a) GIC [A], (b) dH/dt [nT/min], (c) AE index [nT], and (d) SYM-H index [nT] of the geomagnetic event on June 8–9, 2014.

For each of the 11 storm events, visual inspection of the GIC and dH/dt data was performed, similar to that for the event shown in Fig. 8. For the statistical analysis, the distribution of the GICs and geomagnetic variations was plotted for all 31,814 data points. As can be seen in Fig.8, as the amplitude of the variation of dH/dt increases, the GIC data also show large variation. The correlation coefficient was generated to determine the correlation between these two sets of data.

Fig. 9 shows the distribution of GICs for all the storm events. According to this figure, 97.7% of the GICs are within the range of ±1 A; only a very small proportion of the data (2.3%) shows magnitudes >1 A. The maximum range of the GICs is found to be ±7 A. Fig. 10 shows the distribution of dH/dt for all the geomagnetic storm events; it remains within ±5 nT/min for most (99.2%), with only a small proportion of data showing magnitudes >5 nT (0.8%). The maximum range of variation is ±25 nT/min. In other words, for most of the storm events, the domestic GIC and dH/dt data remain within the range of ±1 A and ±5 nT/min, respectively, except for very rare cases in which the magnitude increases considerably to more than five times the normal value. Using the total GIC and dH/dt data, the correlation between

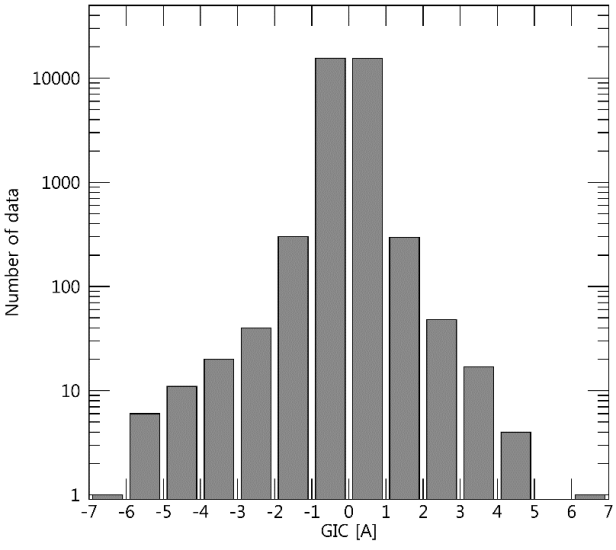

Fig. 9. Distribution of GICs during all geomagnetic storm events.

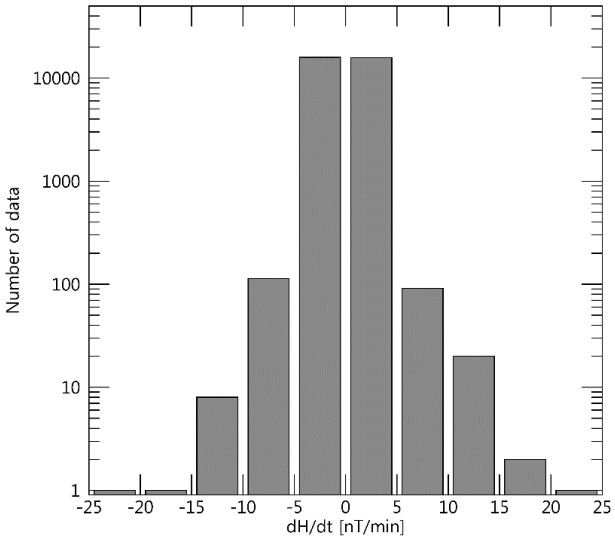

Fig. 10. Distribution of dH/dt during all geomagnetic storm events.

the two data sets was calculated to be -0.516. Although this value indicates an inverse proportionality, it is confirmed quantitatively that the GICs vary considerably when the value of dH/dt is large; the results are shown in Fig. 11. As shown in this figure, GIC and dH/dt fluctuate considerably in very rare cases. Thus, to establish the degree of this variation, the standard deviations of the GIC and dH/dt data on an hourly basis were generated and analyzed. Furthermore, to determine the dependency on specific periods, the same data were generated for 10 min intervals and the results were analyzed.

Fig. 12(a) shows the comparison results of the standard

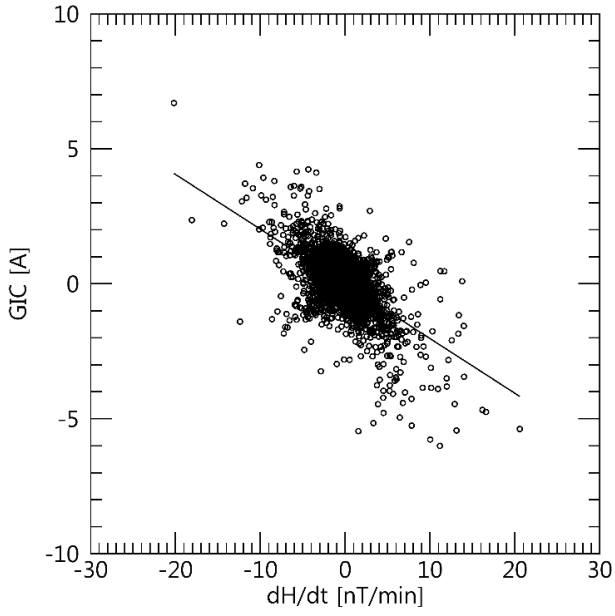

Fig. 11. Correlation of GIC and dH/dt during all geomagnetic storm events.

deviations of GIC and dH/dt data on an hourly basis. The gray plus indicate strong geomagnetic storm events, i.e., periods in which the minimum value of the SYM-H index is < -100 nT. In order to verify that both GIC and dH/dt experience greater variation when geomagnetic storms are strong, the data are overlapped. While the hourly standard deviation of the GIC data is within the range 0–0.4 A for most cases, the maximum deviation is 2 A, i.e., five times greater than the standard deviation. In addition, while most of the standard deviations of dH/dt are within the range 0–1 nT/min, the maximum deviation is 6 nT/min, i.e., six times greater than most cases. Therefore, for most geomagnetic storm events, the fluctuation is almost the same as the average value, but for extremely rare cases, the variation can be up to five times greater than the average. The correlation coefficient of the standard deviation of hourly GIC and dH/dt data was calculated to be 0.89, indicating that the two data sets are well correlated. According to the red circles in Fig. 12(a), for some cases, stronger geomagnetic storms led to a standard deviation. However, the number of samples was insufficient for statistical validity and thus, further analysis of a greater number of strong geomagnetic storms is required. Fig. 12(b) shows the comparison results of the standard deviations of the GIC and dH/dt data on a 10 min basis, the maximum values of the standard deviation of which are 3.2 A and 11 nT/min, respectively. The correlation coefficient was found to be 0.81, which is similar to that of the hourly standard deviation.

For information, the mean values of the GIC and dH/dt on an hourly and 10 min basis were calculated and the results are shown in Fig. 13. In this calculation, the mean value was calculated based on the absolute value to calculate the magnitude. Fig. 13(a) shows the average values of the |GIC| and |dH/dt| on an hourly basis, which are within the range of 0–1.5 A and 0–5 nT/min, respectively. The correlation coefficient was calculated to be 0.88. Fig. 13(b) shows a similar plot on the 10 min basis; the range of the average |GIC| is 0–4 A and that of |dH/dt| is 0–10 nT/min (the correlation coefficient was 0.82).

4. CONCLUSIONS

The details of the installation process of the induced current measurement system at the SINGAPYEONG Substation in 2012 were described; SINGAPYEONG Substation is equipped with 765 kV extra-high-voltage transformers and an induced current measurement system was installed by the KSWC of the RRA. In order to obtain accurate and timely information of induced currents, such as the location, time, and magnitude,

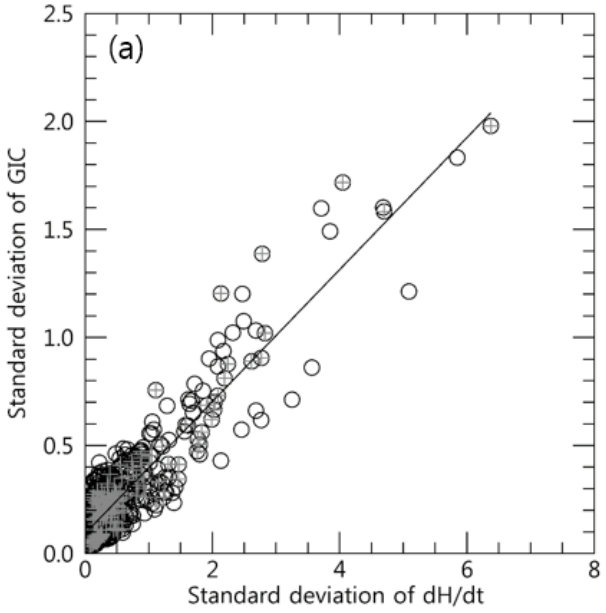

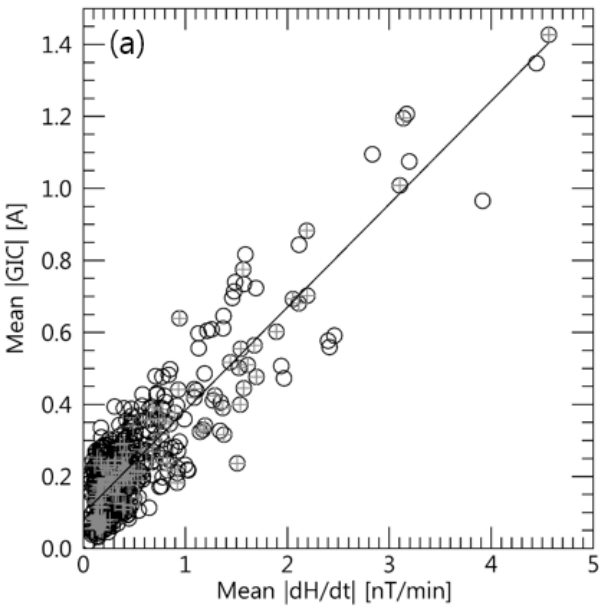

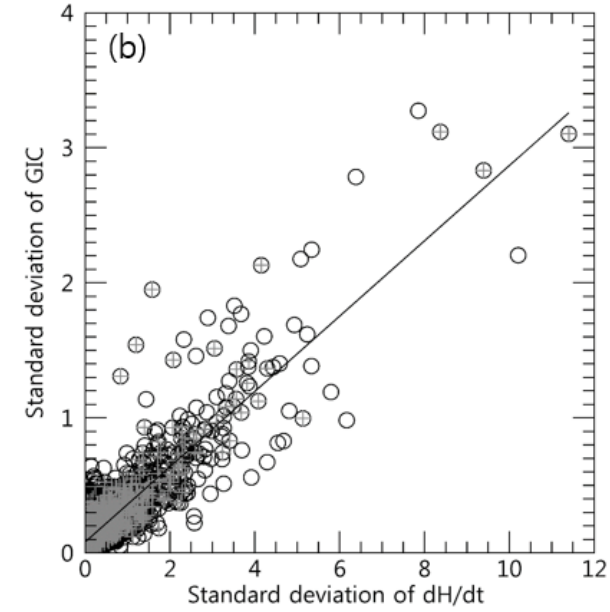

Fig. 12. Correlation of standard deviation of GIC and dH/dt: (a) hourly bias and (b) 10 min bias during geomagnetic storm event.

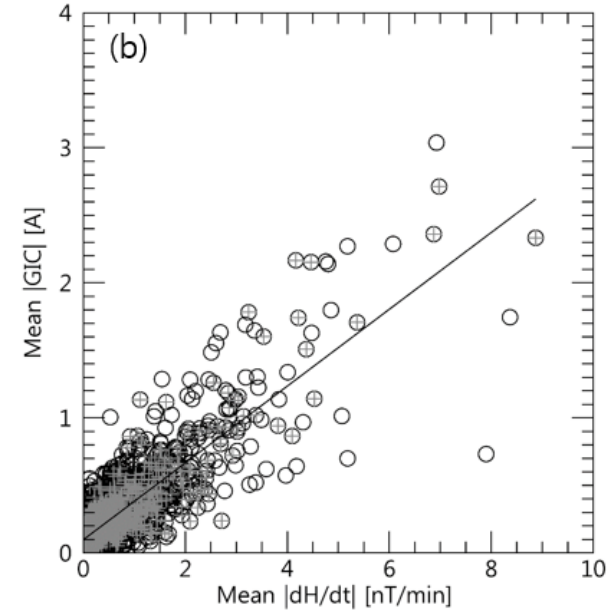

Fig. 13. Correlation of average value of |GIC| and |dH/dt|: (a) hourly bias and (b) 10 min bias during geomagnetic storm events

data from the induced current measurement systems installed at the MIGEUM and SINPOCHEON substations in 2014, were also examined. The measured induced current data, collected by these systems, are stored and analyzed using a data acquisition PC at each substation, as well as being transmitted to the KSWC server at Jeju for monitoring.

The variation of GIC data measured at the SINGAPYEONG Substation and dH/dt data measured at the Icheon geomagnetic observatory during geomagnetic storm periods were compared and analyzed. The results revealed that the hourly standard deviation of GICs during geomagnetic storms was within the range of 0–0.4 A and the maximum deviation was 2 A, which was more than five times greater than the average. The standard deviation of the dH/dt data was within the range of 0–1 nT/min for most cases; however, the maximum deviation observed was 6 nT/min, which was over six times greater than the average. The correlation coefficient between the GIC and dH/dt data sets was calculated to be 0.89 and their degree of variation over time almost matched each other. For further analysis, the effects of such variations on domestic power grids will be studied by

including a greater number of geomagnetic storm events and quiescent periods for comparative analysis.

ACKNOWLEDGMENTS

This work was supported by the "Development of GIC (Geomagnetic Induced Current) Integrated Analysis Technology" project of the Korean Space Weather Center (KSWC).

REFERENCES

Ahn BH, Space Environment Physics *in Korean* (Sigma Press, Seoul, 2000), 142-145.

Boteler DH, Space Weather Effects on Power Systems, in Space Weather, vol. 125, Geophysical Monograph Series, eds. Song P, Singer HJ, Siscoe GL (AGU, Washington, D.C., 2001), 347–352.

Boteler DH, Shier RM, Watanabe T, and Horita RE, Effects of geomagnetically induced currents in the B.C. Hydro 500 kV system, IEEE Trans. Power Delivery 4, 818-823 (1989). http://dx.doi.org/10.1109/61.19275

Cho KS, Moon YJ, Kim YH, Choi SW, Kim RS, et al., Effects of Solar Activity and Space Environment in 2003 Oct., J. Astron. Space Sci. 21, 315-328 (2004). http://dx.doi.org/10.5140/JASS.2004.21.4.315

Choi KC, Cho KS, Moon YJ, Kim KH, Lee DY, et al., Near real-time Estimation of Geomagnetic local K Index from Gyeongzu Magnetometer, J. Astron. Space Sci. 22, 431-440 (2005). http://dx.doi.org/10.5140/JASS.2005.22.4.431

Kappenman JG, An Introduction to Power Grid Impacts and Vulnerabilities from Space Weather, in Space Storms and Space Weather Hazards, vol. 38, NATO Science Series, ed. Daglis IA (Kluwer Academic Publishers, Norwell, 2000), 335–361.

Kappenman JG, Albertson VD, Mohan N, Current Transformer and Relay Performance in the Presence of Geomagnetically-Induced Currents, IEEE Trans. Power Apparatus Syst. PAS-100, 1078-1088 (1981). http://dx.doi.org/10.1109/TPAS.1981.316574

Kim JH, Chang HY, Statistical Properties of Geomagnetic Activity Indices and Solar Wind Parameters, J. Astron. Space Sci. 31, 149-157 (2014). http://dx.doi.org/10.5140/JASS.2014.31.2.149

Kim JH, Lee DY, Choi CR, Her YT, Han JW, et al., Statistical Relationship between Sawtooth Oscillations and Geomagnetic Storm, J. Astron. Space Sci. 25, 157-166 (2008). http://dx.doi.org/10.5140/JASS.2008.25.2.157

Moon YJ, Choe GS, Wang H, Park YD, Gopalswamy N, et al., A Statistical Study of Two Classes of Coronal Mass Ejections, Astrophys. J. 581, 694-702 (2002). http://dx.doi.org/10.1086/344088

Oh SY, Kim BG, Variation of Solar, Interplanetary and Geomagnetic Parameters during Solar Cycles 21-24, J. Astron. Space Sci. 30, 101-106 (2013). http://dx.doi.org/10.5140/JASS.2013.30.2.101

Park SW, Analysis research of geomagnetic field and the domestic power grid induced currents correlation, RRA research report (2013).

Park SW, Ryu CH, Electric grid induced electric field prediction value verification caused by geomagnetic disturbances, RRA research report (2013).

Park WY, Lee JW, Yi Y, Ssessanga N, Oh SY, Storm Sudden Commencements Without Interplanetary Shocks, J. Astron. Space Sci. 32, 181-187 (2015). http://dx.doi.org/10.5140/JASS.2015.32.3.181

Rho SL, Chang HY, Comparing Directional Parameters of Very Fast Halo CMEs, J. Astron. Space Sci. 25, 383-394 (2008). http://dx.doi.org/10.5140/JASS.2008.25.4.383

Rho SL, Chang HY, Relations Among Sunspots, CMEs and Geomagnetic Storms in Solar Cycle 23, J. Astron. Space Sci. 26, 9-24 (2009).

Sung SK, Lee DH, Propagation of CME in Multi-Satellite Observations, J. Astron. Space Sci. 15, 307-320 (1998).

Wang YM, Ye PZ, Wang S, Zhou GP, Wang JX, A statistical study on the geoeffectiveness of Earth-directed coronal mass ejections from March 1997 to December 2000, J. Geophys. Res. 107, 1340 (2002). http://dx.doi.org/10.1029/2002JA009244